International Journal of Applied and Natural Sciences (IJANS)
ISSN(P): 2319-4014; ISSN(E): 2319-4022
Vol. 4, Issue 4, Jun - Jul 2015, 31-38

International Academy of Science, Engineering and Technology
Connecting Researchers; Nurturing Innovations

STRUCTURAL AND ELECTRICAL STUDIES ON CU-MN NANOPARTICLES FERRITES

M. H. MAHMOUD[1], H. AHMED[2], R. GABR[3] & M. M. HAFIZ[4]

[1,2]Physics Department, Faculty of Science & Arts, Al jouf University, Al Guroyat, Saudi Arabia

[2,4]Department of Physics, Assiut University, Assiut, Egypt

[3]Department of Chemistry, Assiut University, Assiut, Egypt

ABSTRACT

A series of nanometer-size $Cu_xMn_{1-x}Fe_2O_4$ ferrite samples, with (x=0.0, 0.2, 0.4, 0.6, 0.8, 1) were prepared using the co-precipitation method. The samples were synthesized with varying calcinations temperature over the range of 600–1275^oC. The synthesis conditions have strongly influenced on the crystal structure, crystallite size, microstructure, and electrical properties. The powders obtained were characterized by X-ray diffraction (XRD) and Fourier transformation infrared (FTIR) spectroscopy. For the crystalline structure investigated, single cubic spinel is gained when the precursor was decomposed at 800–1000 ^oC, whereas separated crystal CuO formed when calcinations temperature is below 800. The IR absorption spectra analyses were used for the detection and confirmation of the chemical bonds in spinel ferrites. The D.C. electrical conductivity of the samples was measured as a function of temperature. The temperature, and time of reaction during synthesis has been shown to play a deterministic role in obtaining the semiconducting oxide in the required size regime with improved.

KEYWORDS: Nanoparticles, Ferrites, Infrared Spectroscopy, DC Electrical Measurements

INTRODUCTION

Nanoparticle ferrites are among the most important magnetic materials that can be widely used in many fields. Finite-size and surface effects, in addition to changes in the degree of inversion, cause nanoferrites to display novel magnetic behaviors[1-3].By virtue of magnetic and semi-conducting properties, Cu ferrite ($CuFe_2O_4$) and its solid solutions with other ferrites are widely used in electronic industry. Moreover, ferrites have gained more importance because they possess the combined properties of magnetic materials and insulators.

It is a well-known fact that the properties of ferrite materials are strongly influenced by the material's composition and microstructure, which are sensitive to the preparation method used in their synthesis [4]. In addition, the sintering conditions employed and the impurity levels present in or added to these materials also change their properties [5,6].

The present investigation is devoted to the study of the physical and structural properties of the$Cu_xMn_{1-x}Fe_2O_4$, where (x=0.0, 0.2, 0.4, 0.6, 0.8, 1) prepared by the low temperature co-precipitation route. The samples are investigated using X-ray, Fourier transforms infrared (FTIR) spectroscopy and the D.C. electrical conductivity.

Experimental

The proposed Cu-Mn ferrite was prepared by co-precipitation method using pure materials: copper nitrates, iron nitrates, and manganese nitrate solution in molar ratios. These materials were dissolved in distilled water separately and then added together. After that one mole of NaOH was dissolved in 1 L of distilled water and added to the dissolved salts

slowly with vigorous stirring till all metal cations precipitated. The pH of the final slurry was carefully adjusted to 10. The precipitate was filtered and washed with distilled water and allowed to dry in furnace at 110^0C. This method was successfully used to prepare samples with the chemical formula, $Cu_{1-x}Mn_xFe_2O_4$, the prepared samples were heated in a muffle furnace at 600, 700 and 800 ^{0}C for 5 h. The sample sannealed at (1275, 1275, 1250, 1250, 1050, 1050) ^{0} C for (x=0.0, 0.2, 0.4, 0.6, 0.8, 1), respectively for about 12 h.

X-ray powder diffractograms were recorded, Cu K_α radiation (λ=1.541838 Å) was used as a constant source of radiation. The generator was operated at 35 KV and 20 mA. Infrared (IR) spectroscopic study was performed in the present study in the range 400-4000 cm^{-1}.The DC conductivity measurements were done using two-probe method.

RESULTS AND DISCUSSIONS

X-ray Diffraction

Phase formation of the Mn-Cu ferrite nanoparticles at different calcinations temperatures was proved by XRD studies. As shown in Figure 1, the broadening of XRD peaks indicate the nanometric crystallite size of the prepared samples. The broadening of the peaks decreased with increasing temperature, which means that the particle size increase.

The XRD data were analyzed using full-prof refinement and the obtained phases formed in different samples at different calcinations temperature, the lattice parameters and space groups were summarized in Table 1. Full profile fitting including a base line of the diffraction patterns were done assuming pseudo Lorentzian line shape, which accounts for the asymmetry for each peak, from which the Bragg angle, peak intensity, and the angular width at half maximum intensity were determined [3]. The crystallite size (D) was estimated from XRD line broadening after accounting for the instrumental broadening using Scherrer method and the data were given in Table1.

Figure 2 shows the relation between the lattice constant and particle size with temperature for the composition $Mn_{0.4}Cu_{0.6}Fe_2O_4$, which is similar for all the other samples. As shown, the mean crystallite size increase, while the lattice constant decrease with increasing of calcinations temperature. The lattice expansion corresponds to a negative pressure that was probably produced by the strong repulsive interaction of the parallel surface defect magnetic dipoles at small particle sizes. Similar nanoscale lattice modifications have been observed in other magnetic systems [7, 8]. A possible rearrangement of Fe^{3+}, Cu^{2+}, Mn^{3+} ions between the tetrahedral and octahedral sites takes place. This variation in the structure might play a signification role in controlling both the magnetic parameters and the sample resistivity [9].

IR - Spectroscopy

Infrared spectra of the copper manganese ferrite samples were analyzed in the frequency range (400-4000) cm^{-1}. Figure 3 shows the FTIR spectra of $Cu_xMn_{1-x}Fe_2O_4$ (x=0.0, 0.2, 0.4, 0.6, 0.8, 1) calcined at different temperatures. The existence of the characteristic bands of NO^{-3} at 1300 cm^{-1} indicated that the NO^{-3} as a group exists in the structure of the mixed solution formed from metal nitrates. The bands at 1600 cm^{-1} and the broad feature between 3500 and 3600 cm^{-1} are ascribed to stretching modes H–O–H bending vibration of the residue water [10]. It is corresponds to the hydroxyl groups attached by the hydrogen bonds to the iron oxide surface and the water molecules chemically adsorbed to the magnetic particle surface (associated water content) [11]. The strength of the IR absorption bands corresponding to O-H group, carboxyl group and NO_3^{-1}, disappeared completely by increasing the sintering temperature. The disappearances of the characteristic bands of NO_3^{-1}ion in the spectra suggests that NO_3^{-1}ions take part in the reaction and are almost burnt out during the process.

The two absorption bands below 1000 cm^{-1} seen in the spectra are characteristic of all spinel ferrites [12]. The first frequency band $\nu_1$at around (569-541) cm^{-1} and the second frequency band $\nu_2$at around (413-400) were assigned to tetrahedral T_d and octahedral O_h sites, respectively. The broadening is commonly observed for inverse spinel ferrites, which is attributed to the statistical distribution of Fe at A and B sites. The ν_1 band continues to shift towards the higher values by increasing Cu^{2+} concentrations for all the calcined samples, which agree with previous studies [13]. It is known that the frequency is inversely proportional to reduced mass and bond length [14]. The shift of lattice vibration to the higher frequency could be attributed to the difference in the ionic radius and masses between Cu^{2+}(0.70Å) and Mn^{2+} (0.91Å) ions. In this composition some Cu^{2+} ions are replaced by manganese ions which have smaller atomic mass than that of Cu^{2+}. Thus total mass of the lattice decreases leading to an increase in band frequency.

The frequency band values ν_1 decrease with increasing the calcinations temperatures. This variation could be attributed to a different cation distribution. A previous study showed that the frequency band values $\nu_2$of the $MnFe_2O_4$ nanoparticles is about 379 cm^{-1} [15]. However, due to the limitation of our FTIR instrument, bands below 400 cm^{-1} were not detected clearly.

Electrical Measurements

The DC electrical resistivity for all the samples was measured in a temperature range 100 to 400 ^{0}C. The variation of D.C. resistivity as a function of reciprocal of temperature is shown in Figure 4. The samples show semiconducting behavior, where the D.C. electrical resistivity shows a linear decrease with increase in temperature. The resistivity in ferrites obeys the relation,

$$\rho = \rho_0 \exp(E_g / KT)$$

where E_g represent the thermal activation energy, K is Boltzmann's constant, ρ_0 is the specific resistivity at absolute zero temperature, ρ is the specific resistivity at temperature T, and T is absolute temperature.

The variation of dc-electrical resistivity of ferrites can be explained on the basis of Verway hopping mechanism [16].According to this mechanism, hopping of electrons play a technical role in electrical conduction of ferrites between the ions of same element, with different valence states present at octahedral sites [17]. Creation of Fe^{2+} ions gives rise to electron hopping between the Fe ions in +2 and +3valence states. The hopping probability depends upon the separation between the ions involved and the activation energy, which is associated with the electrical energy barrier experienced by the electrons during hopping. However, the decrease in resistivity also may be attributed to the fact that in case of Mn-doped copper ferrite octahedral sites are occupied by Cu^{2+}, Fe^{3+} and Mn^{4+} ions [18]. A systematic study of the cation distribution in Cu substituted manganese ferrites has been made by Rana et. al [19]. They concluded that these ferrites belong to the family of mixed or partially inverse spinel. This conclusion is matched with our FTIR results. The activation energy of each sample in table 2 is calculated from the plots of logρ versus 10^3/T. It lies within the range 0.53 to 0.89 eV. The activation energy increases with increase in cu content. The increasing values of particle size with increasing calcinations temperature also contribute to lower the resistivity which may be due to the decrease in the activation energies.

CONCLUSIONS

The results can be summarized as follows:

- Copper – Manganeseferrite nanoparticles have been synthesized via the co-precipitation method with the chemicalformula $Cu_{1-x}Mn_xFe_2O_4$, with (x=0.0, 0.2, 0.4, 0.6, 0.8, 1).
- X-ray analysis confirmed the formation of the single phasefor the compositions x = 0 and 0.2when the samples heated at1275^oC, while the other concentrations x = 0.4 and 0.6 formed at 1250^oC and the concentrations x = 0.8 and 1 formed at 1050^oC.
- The lattice parameters decrease with increasing the calcinations temperature while the mean crystallite size increases.
- The IR spectral measurements indicate the presence of two fundamental absorption bands $\nu_1$and ν_2 which are found in theexpected range for a spinel type ternary oxide.The slight increase of ν_1 with increasing Cu^{2+}could be attributed tothe difference in the ionic radius between Cu^{2+} and $Mn^{2+}$and the difference of their masses in the A-site.
- The DC electrical conductivity increases with increasing temperature, which is a normal characteristic of semiconductor ferrites. This increase in the conductivity could be related to the increase in the drift mobility of the charge carriers, which are localized at ions or vacant sites.
- The increase in copper content leads to a decrease in hopping length (L) and hence facilitates the electron hopping between Fe^{2+} and Fe^{3+} states at the B sites, and in turn leads to increase in the activation energy and electrical conductivity.

REFERENCES

1. M.H. Sousa, F.A. Tourinho, J. Depeyrot, G.J.D. Silva, M.C.F.L. Lara, J. Phys. Chem. B 105 (2001) 1168.
2. N. Kasapoglu, A. Baykal, Y. Koseoglu, M.S. Toprak, Scripta Mater. 57(2007) 441.
3. S. Yu, M. Yoshimura, Chem. Mater. 12 (2000) 3805.
4. P.S. Anilkumar, J.J. Shrotri, S.D. Kulkarni, C.E. Deshpande,S.K. Date, Mater. Lett. 27(1996) 293.
5. B.P. Rao, P.S.V.S. Rao, P. Rao, IEEE Trans. Magn. 33 (6) (1997) 4454.
6. R. Iyer, R. Desai,R.V. Upadhyay,Bull. Mater. Sci. 32 (2009) 141.
7. R.D. Shannon, Acta crystallographica A 32 (1976) 751.
8. A.H. Morrish, "The physical principles of magnetism", IEEE press, New York (2001).
9. F.X. Cheng. J.T. Jia, Z.G. Xu, B. Zhou, C.S. Liao, C.H. Yan, L.Y. Chen, H.B. Zhao, J. Appl. Phys. 86 (1999) 2727.
10. M. Bahout, S. Betrand, O. Pena, J. Solid State Chem. 178 (2005) 1080.
11. S. Maensiri, C. Masingboon, B. Boonchom, S. Seraphin, Scr. Mater. 56 (2007) 797.
12. M.H. Mahmoud, M.I. Abd-Elrahman, Materials Letters 73 (2012) 226.
13. L.M. Salah, A.M. Moustafa , I.S. Ahmed Farag , Ceramics International 38 (2012) 5605.

14. M.A. Amer, A.Tawfik , A.G.Mostafa , A.F.El-Shora, S.M.Zaki, J. Magnetism &Magnetic Materials 323 (2011) 1445.
15. R.K. Selvan, C.O. Augustin, L.B. Berchmans, R. Sarawathi, Res. Bull. 38 (2003) 41.
16. E.J. Verway, P.W. Haayman, F.C. Romejn, J.Chem. Phys. 15 (1994)187.
17. E.1. W. Verwey and J. H. de Boer, Rec. Trav. Chim. Phys. Bas., 55 (1936) 531.
18. Yue, Jizhou, Zhilum Gui, Longtu Li, J. Mag. Mag. matter 264 (2003) 258.
19. M.U.Rana , Misbah-Ul-Islam, Abbas T.J. Material science 38 (2003) 2037.

APPENDICES

Table 1: Summary of the Phases and Structure Parameters for $Cu_xMn_{1-x}Fe_2O_4$ (x=0.0, 0.2, 0.4, 0.6, 0.8, 1) at Different Calcinations Temperatures

samples	Annealing Temperature (^{0} C)	Lattice Constants (^{0}A)	Mean Crystallite size(D) (nm)	β_{ins} (rad.)	Phases		
					Phase 1	Phase 2	Phase 3
$MnFe_2O_4$	600	8.55403	7.26034	0.000248	Mn ferrite	Mn_5O_8	Fe_2O_3
	700	8.54511	14.09969	0.033314	Mn ferrite	Mn_5O_8	Fe_2O_3
	800	8.48755	8.124267	0.013540	Mn ferrite	-	Fe_2O_3
	1275	8.44889	29.11765	0.001125	Mn ferrite	-	Fe_2O_3
$Cu_{0.2}Mn_{0.8}Fe_2O_4$	600	8.54269	18.28496	0.000620	(Cu-Mn) ferrite	Mn_5O_8	Fe_2O_3
	700	8.48052	15.78588	0.000524	(Cu-Mn) ferrite	Mn_5O_8	Fe_2O_3
	800	8.46842	24.53097	0.000876	(Cu-Mn) ferrite	Mn_5O_8	Fe_2O_3
	1275	8.45702	98.29787	0.001582	(Cu-Mn) ferrite	Mn_5O_8	Fe_2O_3
$Cu_{0.4}Mn_{0.6}Fe_2O_4$	600	8.49411	4.507317	0.032881	(Cu-Mn) ferrite	Mn_5O_8	Fe_2O_3
	700	8.46854	20.08969	0.000996	(Cu-Mn) ferrite	Mn_5O_8	Fe_2O_3
	800	8.48071	18.9863	0.00135	(Cu-Mn) ferrite	Mn_5O_8	Fe_2O_3
	1250	8.40974	28.63636	0.0019	(Cu-Mn) ferrite	-	-
$Cu_{0.6}Mn_{0.4}Fe_2O_4$	600	8.49407	2.652632	0.026941	(Cu-Mn) ferrite	Mn_5O_8	Fe_2O_3
	700	8.44349	19.54866	0.001674	(Cu-Mn) ferrite	Mn_5O_8	Fe_2O_3
	800	8.43996	26.00375	0.000941	(Cu-Mn) ferrite	Mn_5O_8	Fe_2O_3
	1250	8.41384	30.52863	0.002543	(Cu-Mn) ferrite	-	-
$Cu_{0.8}Mn_{0.2}Fe_2O_4$	600	8.49356	3.616191	0.032611	(Cu-Mn) ferrite	Mn_5O_8	Fe_2O_3
	700	8.41577	9.130435	0.007584	(Cu-Mn) ferrite	Mn_5O_8	Fe_2O_3
	800	8.40367	4.998197	0.022342	(Cu-Mn) ferrite	-	Fe_2O_3
	1050	8.41213	66.63462	0.001462	(Cu-Mn) ferrite	-	-
$CuFe_2O_4$	600	8.46456	10.811234	0.011011	Cu ferrite	CuO	Fe_2O_3
	700	8.4545	21.063833	0.001091	Cu ferrite	CuO	Fe_2O_3
	800	8.40687	29.806451	0.000996	Cu ferrite	-	Fe_2O_3
	1050	8.4022	78.654985	0.002648	CU ferrite	-	-

Table 2: The Energy Gap Values of the $Cu_xMn_{1-x}Fe_2O_4$ Nanoparticles at Different Calcinations Temperatures

Composition	Energy Gap in ev		
	600 c	700 c	800 c
$MnFe_2O_4$	0.53	0.63	0.78
$Cu_{0.2}Mn_{0.8}Fe_2O_4$	0.77	0.76	0.81
$Cu_{0.4}Mn_{0.6}Fe_2O_4$	0.57	0.75	0.89
$Cu_{0.6}Mn_{0.4}Fe_2O_4$	0.67	0.79	0.71
$Cu_{0.8}Mn_{0.2}Fe_2O_4$	0.86	0.87	0.85
$CuFe_2O_4$	0.66	0.68	0.89

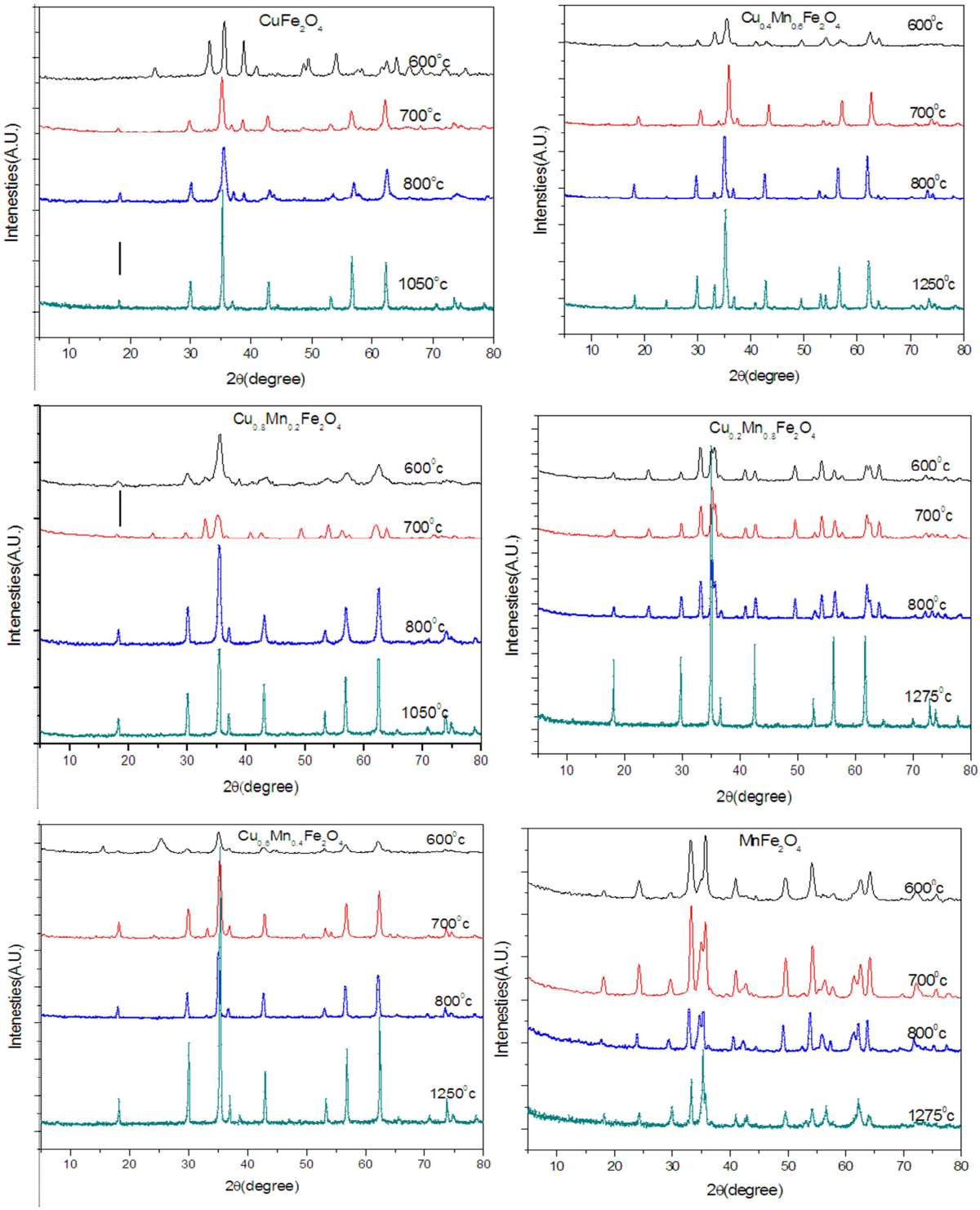

Figure 1: X-ray Diffraction Pattern of $Cu_xMn_{1-x}Fe_2O_4$, where (x=0.0, 0.2, 0.4, 0.6, 0.8, 1) at Different Calcinations Temperatures

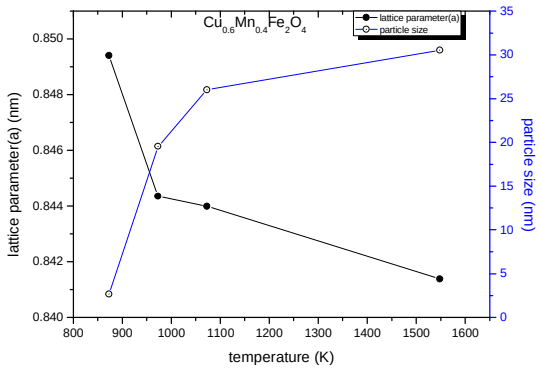

Figure 2: Lattice Constant and Particle size of $Cu_{0.6}Mn_{0.4}Fe_2O_4$ Nanoparticles as a Function of Temperature

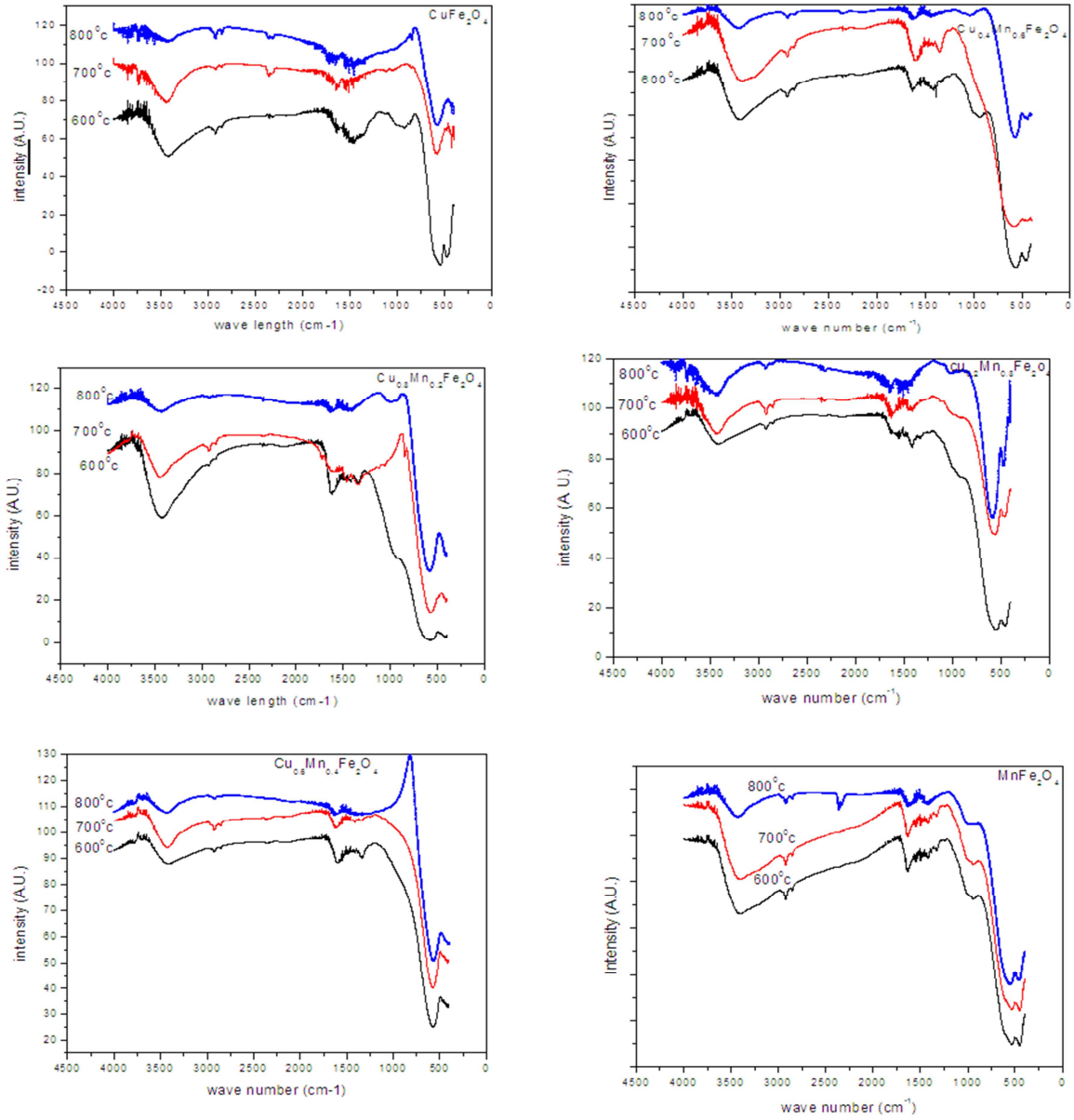

Figure 3: FTIR Spectra of $Cu_xMn_{1-x}Fe_2O_4$ (x=0.0, 0.2, 0.4, 0.6, 0.8, 1) Calcined at Different Temperatures

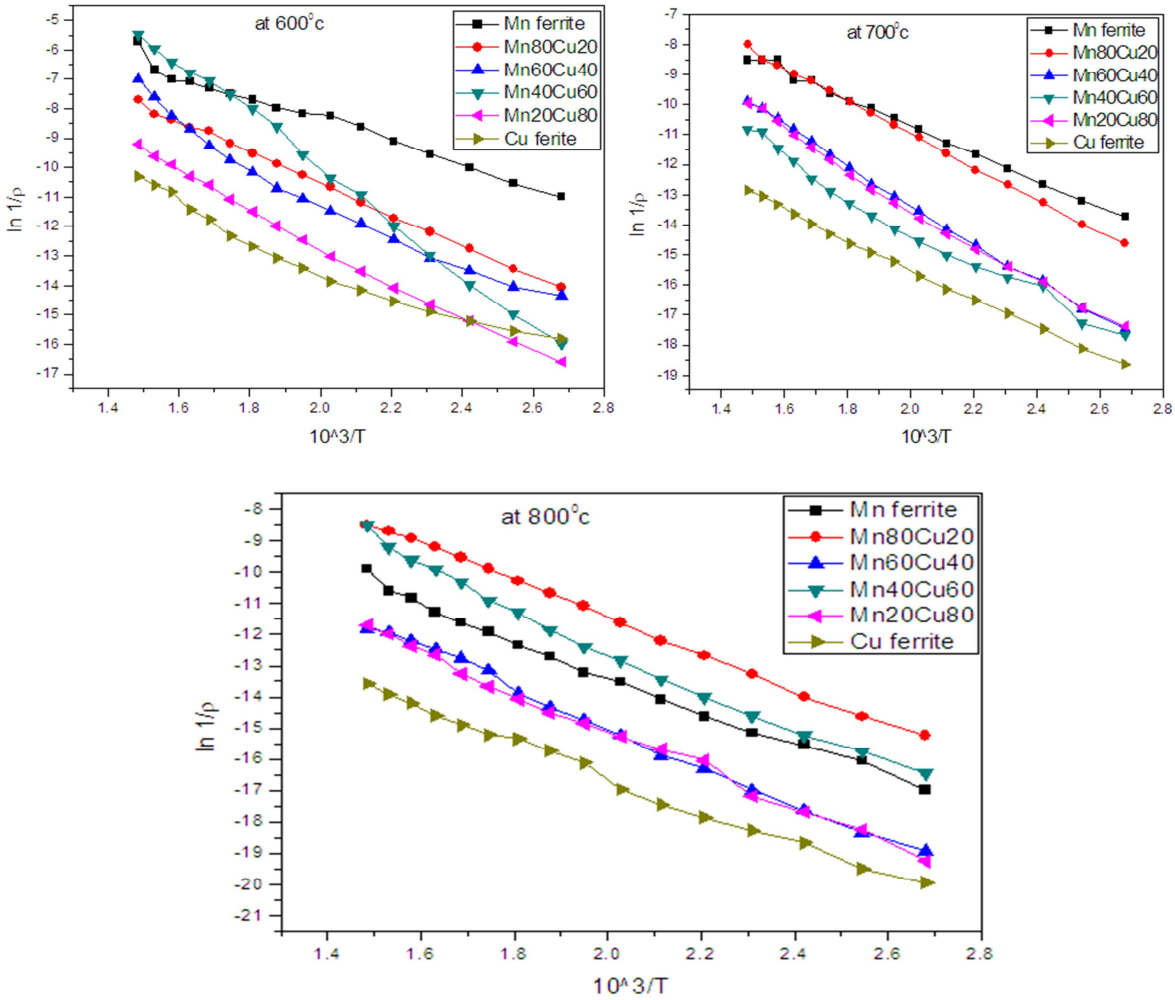

Figure 4: Variation of DC Electrical Resistivity of $Cu_xMn_{1-x}Fe_2O_4$ calcinied at (600, 700 and 800^{0}c) as a Function of Temperature